Low-cost Fourier ghost imaging using a photoresistor

Ritz Ann P. Aguilar,* Nathaniel Hermosa, and Maricor N. Soriano

National Institute of Physics, University of the Philippines Diliman, Quezon City, Philippines
*Corresponding author: raguilar@nip.upd.edu.ph

Abstract

Computational ghost imaging is a novel way of digital imaging using a single photodetector by obtaining spatial correlations between a scene and a structured pattern illuminating it. In most cases, spatial light modulators (SLMs) and high-quality photodiodes used to do ghost imaging are quite expensive, therefore, limiting its implementation in undergraduate and even graduate optics experiments. Here, we present a cost-effective and easy-to-build ghost imaging setup that addresses this issue by employing a commercial projector and a light-dependent resistor. These are much cheaper and easy-to-find optical instruments. Furthermore, an Arduino-based system is built to automate data gathering and Fourier ghost imaging was used to process the data. Our initial results show that we can have good reconstruction of the object even with the use of low-cost devices.

Keywords: ghost imaging, single-pixel imaging

1 Introduction

Since the development of digital cameras, an array of sensors contained in a charge-couple device (CCD) or a complementary metal oxide semiconductor (CMOS) is being used for imaging. These sensors are composed of photodetectors, which sense an electromagnetic (EM) radiation in the form of resistance, current, and the like, depending on the type of sensor [1]. With each sensor corresponding to one pixel in an image, the usual selling point in a digital camera is the number of pixels it has, i.e. the higher, the better. Working in the non-visible regime, e.g. ultraviolet, the cost of production of the sensors would scale up and for roughly the same resolution, an ultraviolet camera may actually cost far more than that of a camera for the visible regime [2].

One of the very first demonstrations of ghost imaging (GI) was with the concept of two-photon quantum entanglement [3]. Spatial correlations, specifically position, between photon pairs (signal and idler) produced by parametric down conversion were used in an imaging system with detectors having no direct information about the object to be imaged. Since then, GI has developed from quantum to classical to computational. In classical GI, beam pairs produced using a beam splitter from a classical light source are used instead of photon pairs, producing higher correlation strength [4]. Complicated patterns are projected onto the object and their overlap degree is used to determine the correlation strength and subsequently, to reconstruct the object [5].

The elimination of the scanning detector and the beam splitter in quantum and classical GI by introducing a spatial light modulator (SLM) paved way for the emergence of computational GI [6]. Structured patterns are programmed with the SLM and the computer simply obtains the spatial correlation between the pattern and the object. This is, by far, the simplest GI setup that has been proposed in the recent years. In general, GI has a broad spectral range, hence, it has been used in many interesting applications which include imaging of space objects [7] and x-ray tomography [8].

Non-line of sight imaging with high signal-to-noise (SNR) has also been demonstrated through ghost imaging in the Fourier domain [9]. A set of at least three sinusoidal patterns for a single intensity measurement is used for elimination of background noise. Despite this, the algorithm is still fast compared to other GI techniques since it utilizes the idea that images are sparse in the Fourier domain and that most of their information is concentrated in low spatial frequencies. Hence, it is enough to sample the low frequencies to get a general image of the object.

In this paper, we demonstrate a low-cost and easy-to-use Fourier ghost imaging (FGI) setup which may be used in undergraduate physics labs. A light-dependent resistor (LDR) is used instead of a photodiode as a bucket detector. Instead of using an SLM to produce the structured patterns, we simply use a commercial DLP projector. For the analog-to-digital conversion (ADC) of the signal obtained by the LDR, a simple Arduino is used. Finally, the system is automated using Arduino software and Matlab.

2 Theory of Fourier Ghost Imaging (FGI)

Sets of sinuosoidal patterns are used in Fourier ghost imaging (FGI). The intensity of a sinusoidal pattern with pixel coordinates (x, y) and corresponding spatial frequency coordinates (f_x, f_y) is

$$I_n(x, y; f_x, f_y) = a + b \cdot \cos\left[2\pi(f_x x + f_y y) + n \cdot \Delta\phi\right], \tag{1}$$

where a is the DC term (average image intensity), b is the sinusoid amplitude (contrast), and $\Delta\phi$ is the phase shift. Three-bucket algorithm is employed to increase the signal-to-noise ratio (SNR) of the system wherein the phase shift was set to $\Delta\phi = 2\pi/3$ $(n = 0, 1, 2)$. For one pattern, the total intensity of reflected light is

$$E_n(f_x, f_y) = \iint_\Omega R(x, y) I_n(x, y; f_x, f_y) dx dy, \tag{2}$$

where $R(x, y)$ represents the surface reflectivity of the target scene and Ω is the overall illuminated area. The reflected light is then recorded by the single-pixel detector with a total response of $S_n(f_x, f_y) = S_r + kE_n(f_x, f_y)$, where S_r is the background illumination response and k is a simple scaling factor dependent on the size and orientation of the detector.

By scanning through several spatial frequencies for each set of patterns (I_0, I_1, and I_2), we are able to obtain the complex Fourier coefficient $C(f_x, f_y)$, in spatial frequency coordinates as follows:

$$\begin{aligned} \frac{1}{3}\left[2S_0 - S_1 - S_2\right] + \frac{\sqrt{3}}{3} j\left[S_2 - S_1\right] &= bk \iint_\Omega R(x, y) \cdot \{\cos\left[2\pi(f_x x + f_y y)\right] - j \sin\left[2\pi(f_x x + f_y y)\right]\} dx dy, \\ C(f_x, f_y) &= bk \iint_\Omega R(x, y) \cdot \exp\left[-j2\pi(f_x x + f_y y)\right] dx dy \propto \mathcal{F}\{R(x, y)\}. \end{aligned} \tag{3}$$

Taking the inverse Fourier transform of the Fourier spectrum $C(f_x, f_y)$ in Eq. 3, we then recover the image of the scene, $\bar{I}(x, y)$, in pixel coordinates:

$$R(x, y) = \frac{1}{bk} \cdot \mathcal{F}^{-1}\left\{\frac{1}{3}\left[2S_0 - S_1 - S_2\right] + \frac{\sqrt{3}}{3} j\left[S_2 - S_1\right]\right\} \propto \bar{I}(x, y). \tag{4}$$

3 Simulation and Experiment

Numerical simulations were first carried out for the FGI algorithm. A simple binary image as shown in Fig. 2a with a size of 256×256 pixels is used as a test object. The simulation was conducted using Matlab 2014a on an Intel i7 2000-MHz laptop with a 64-bit Windows 8.1 system and 16GB RAM. We set the spectral coverage (SC) to 1%, 10%, 25%, and 100% of the entire Fourier spectrum. Typical parameters used to evaluate the quality of images such as structural similarity index (SSIM) and root-mean-square error (RMSE) were used to compare the reconstruction quality with that of the original image. Both parameters have a range of $[0, 1]$. Higher SSIM or lower RMSE means better image quality.

Four stages were involved in the experiment: (1) building the lux meter, (2) sensor characterization, (3) GI system calibration, and (4) testing and data gathering. A 12 mm × 10 mm × 2 mm Cadmium Sulfide (CdS), typically found in street lamps, whose resistance decreases as light intensity increases was used in this study [1]. In building the lux meter, we made a simple voltage divider for direct conversion of LDR resistance to voltage. The configuration gives an output voltage $V_{\text{out}} = V_{\text{in}} \frac{R_2}{R_1 + R_2}$, where R_1 is the LDR's resistance, $R_2 = 10\,\text{k}\Omega$, and $V_{\text{in}} = +5\,\text{V}$ (from the Arduino).

Time constant, τ, is a characteristic of sensors which defines the time it takes for a sensor to reach 63% of its steady-state value during rise time or 37% during fall time [10]. For the first part, the time constant of the LDR (τ_{LDR}) was obtained by illuminating it with a blinking LED driven by a square wave frequency. The frequency was set to 60 Hz to mimic the refresh rate of the DLP projector. We found out that $\tau_{\text{LDR}} = 5\,\text{ms}$. The capturing time of the LDR for each pattern is then set to $5 \times \tau_{\text{LDR}}$ (25 ms), which gives enough time for the voltage to reach steady-state.

For the second part, the DLP projector was used to project different grey levels ($\propto$ lux) on a white A3 paper while the LDR voltage for each grey level is recorded. This was repeated for 10 trials. Fig. 1 (right) shows the resulting calibration curve with error bars from the standard deviation of all trials of the GI system. In general, we see that it has a nonlinear curve that is most sensitive (steep curve) at low grey levels (low lux) and least sensitive at high grey levels (high lux). Hence, we forced a dark illumination area by setting up a dark background for the object and no other light source apart from the projector was turned on. We also used low amplitude sinusoids for our patterns by setting $b = 0.5$ in Eq. 1.

Finally, we used the calibrated FGI system for testing actual objects. The image used in the simulation was printed on a photo paper to serve as our object. A schematic diagram of our experiment setup is shown in Fig. 1. The actual illuminated area by the sinusoidal fringes is 5.8 cm × 5.8 cm which was just enough to cover our object.

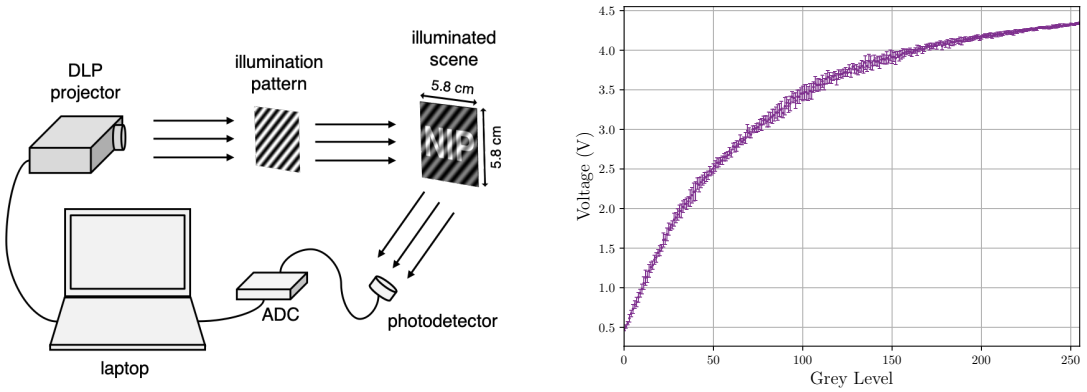

Figure 1: Schematic diagram of the GI divider circuit used for building the lux meter (left). Calibration curve obtained for the FGI system (right).

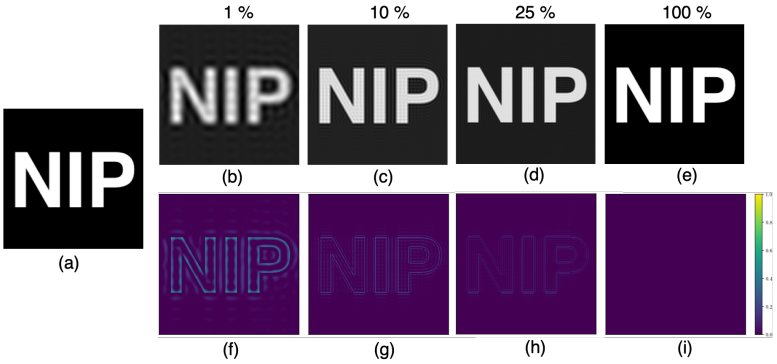

Figure 2: Test image used in the simulation (a). Simulation reconstruction results at different spectral coverage (b-e) and their corresponding error images (f-i).

4 Results and Discussion

Based on the results of the simulations as shown in Fig. 2b to 2e, most of the details of the object were successfully recovered. At 1% SC, we see that the edges were not recovered as shown in Fig. 2f, constituting bulk of the RMSE. There are also fringes or 'ringing effect' at the sides which are caused by artifacts of the shape of the sampling path used (acting like a square filter). The edges are usually high frequencies in the frequency domain which were not sampled since we concentrated on the low frequencies. At 10% and 25% SC, we see more of the edges of the letters N-I-P with the inclusion of higher frequencies. Table 1 shows the SSIM and RMSE values for the simulation results. As expected, SSIM values increase while RMSE decreasease with increasing spectral coverage. At 100% SC, we see that SSIM $= 1$ and RMSE ≈ 0 which means that the algorithm is successful in reconstructing the object.

Due to limited cooling system during the experiment which causes the devices to heat up and the computer to slow down, we limit the imaging to 10% SC wherein reconstructions took approximately 2 hours. Fig. 3 shows us the experiment results obtained at 1% and 10% SC and their corresponding Fourier spectrum. The letters are shifted down since the projected patterns were not fully-centered at the object during projection. The slight distortion in the straight edges of the letters is simply a result of the bulging shape of the object as it was taped onto the scene. No post processing has been done with any of the reconstruction results.

Compared with that of the simulation results for the same SC, we have a much lower image quality which may be attributed to several factors. First, the absence of an optical lens greatly contributed to

Table 1: SSIM and RMSE values obtained from the simulation results.

Parameter	**1%**	**10%**	**25%**	**100%**
SSIM	0.5108	0.8096	0.9178	1
RMSE	0.1172	0.0513	0.0305	9.56×10^{-15}

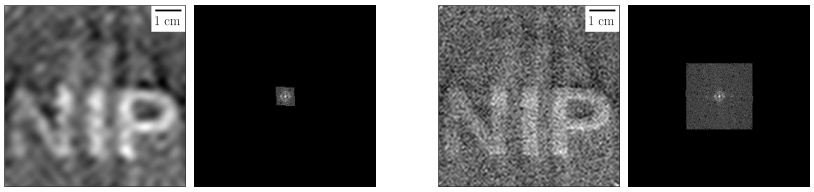

Figure 3: Experiment results with their corresponding Fourier spectrum at 1% (left) and 10% SC (right).

the low image quality since only partial light from the scene is collected by the sensor. Second, the photo paper used has a glossy surface exhibiting back-scattering effects added to the overall intensity. Inspection of Eq. 2 tells that all kinds of incoming light are collected by the detector, hence, the recorded image intensity is affected by the photo paper's reflectivity. Another source of low image quality would be the added noise and distortions in the projected patterns. We assumed that the scene is being illuminated with perfect sinusoids but in reality, environmental noise degrades their quality. Moreover, aliasing occurs at higher frequencies as we go beyond the resolution limit of the projector which causes misindentification of the signal frequency, thus, introducing error with the incorrect mapping of Fourier coefficents. Lastly, limited LDR sensitivity range also affects the contrast of the resulting image since we are only working in the $0 - 50$ grey level regime of the calibration curve.

Despite these factors affecting the reconstruction quality and even at a low SC, we were still able to recover most of the details of the object. The entire setup may be implemented in undergraduate labs provided that the students have basic electronics skills, average-level programming, and knowledge of optics, specifically, 2D Fourier Transforms. To minimize the possible sources of error and to increase the SNR of the system, we recommend using matte test objects as well as placing a lens before the LDR to direct the incoming light from the scene onto its surface. Increasing the illumination area by moving the projector at a farther distance from the scene may offset the effect of aliasing. Playing with different values of R_2 in the voltage divider circuit will change the shape of the calibration curve such that higher sensitivity may be achieved for a larger range of grey levels. The entire FGI system with the inclusion of the laptop only costs around 1500 USD, which is cheaper by around 1000 USD compared to the GI system in [9] and more than $10\times$ cheaper than systems which use SLMs such as in [6].

5 Conclusions and Recommendations

A low-cost automated FGI system was successfully created using relatively cheap optical devices which include an LDR, a commercial projector, an Arduino, and a laptop. To further lessen the cost, a Raspberry Pi (RPi) together with an ADC Integrated Chip may be used to replace both the Arduino and the laptop. Data obtained by the RPi may just be extracted after for further processing. With this alternative, the system would only cost around 450 USD. Both our simulation and experiment results show good reconstruction of the object even with the use of the low-cost devices.

References

[1] W. Flores-Fuentes et al., Comparison between Different Types of Sensors Used in the Real Operational Environment Based on Optical Scanning System, *Sensors* **18**, 1684 (2018).

[2] M. F. Duarte et al., Single-pixel imaging via compressive sampling, *IEEE Signal Process. Mag.* **25**, 83 (2008).

[3] T. B. Pittman, Y. H. Shih, D. V. Strekalov, and A. V. Sergienko, Optical imaging by means of two-photon quantum entanglement, *Phys. Rev. A* **52**, R3429 (1995).

[4] A. Valencia et al., Two-Photon Imaging with Thermal Light, *Phys. Rev. Lett.* **94**, 063601 (2005).

[5] F. Ferri, D. Magatti, L. A. Lugiato, and A. Gatti, Differential Ghost Imaging, *Phys. Rev. Let.* **104**, 253603 (2010).

[6] J. H. Shapiro, Computational ghost imaging, *Phys. Rev. A* **78**, 061802 (2008).

[7] D. V. Strekalov, B. I. Erkmen, and N. Yu, Ghost Imaging of Space Objects, *J Phys Conf Ser* **414**, 012037 (2013).

[8] A. M. Kingston, D. Pelliccia, A. Rack, M. P. Olbinado, Y. Cheng, G. R. Myers, and D. M. Paganin, Ghost tomography, *Optica* **5**, 1516 (2018).

[9] Z. Zhang, X. Ma, and J. Zhong, Single-pixel imaging by means of Fourier spectrum acquisition, *Nat. Commun.* **6**, 6225 (2015).

[10] Y. Kraftmakher, *Experiments and demonstrations in physics* (World Scientific, 2007).